Two-photon imaging of Zn^{2+} dynamics in mossy fiber boutons of adult hippocampal slices

Mustafa Khan[a,1], Christian R. Goldsmith[b,c,1], Zhen Huang[b], John Georgiou[a], Thomas T. Luyben[a,d], John C. Roder[a,d], Stephen J. Lippard[b,2], and Kenichi Okamoto[a,d,2]

[a]Lunenfeld-Tanenbaum Research Institute, Mount Sinai Hospital, Toronto, ON, Canada M5G 1X5; [b]Department of Chemistry, Massachusetts Institute of Technology, Cambridge, MA 02139; [c]Department of Chemistry and Biochemistry, Auburn University, Auburn, AL 36849; and [d]Department of Molecular Genetics, Faculty of Medicine, University of Toronto, Toronto, ON, Canada M5S 1A8

Contributed by Stephen J. Lippard, March 25, 2014 (sent for review January 22, 2014)

Mossy fiber termini in the hippocampus accumulate Zn^{2+}, which is released with glutamate from synaptic vesicles upon neural excitation. Understanding the spatiotemporal regulation of mobile Zn^{2+} at the synaptic level is challenging owing to the difficulty of visualizing Zn^{2+} at individual synapses. Here we describe the use of zinc-responsive fluorescent probes together with two-photon microscopy to image Zn^{2+} dynamics mediated by NMDA receptor-dependent long-term potentiation induction at single mossy fiber termini of dentate gyrus neurons in adult mouse hippocampal slices. The membrane-impermeant fluorescent Zn^{2+} probe, 6-CO_2H-ZAP4, was loaded into presynaptic vesicles in hippocampal mossy fiber termini upon KCl-induced depolarization, which triggers subsequent endocytosis and vesicular restoration. Local tetanic stimulation decreased the Zn^{2+} signal observed at individual presynaptic sites, indicating release of the Zn^{2+} from vesicles in synaptic potentiation. This synapse-level two-photon Zn^{2+} imaging method enables monitoring of presynaptic Zn^{2+} dynamics for improving the understanding of physiological roles of mobile Zn^{2+} in regular and aberrant neurologic function.

zinc ion | metalloneurochemistry

Although most cellular Zn^{2+} is sequestered within proteins, stores of loosely bound Zn^{2+} are present in many kinds of cells. This mobile Zn^{2+} pool is believed to mediate cellular processes, including neurotransmission (1). Within the hippocampus, mossy fibers connecting the dentate gyrus (DG) and the CA3 regions contain Zn^{2+} in glutamatergic synaptic vesicles. The precise concentration of Zn^{2+} within the neuronal vesicles is unknown, with upper estimates ranging in the low millimolar range (2, 3). Upon stimulation, Zn^{2+} is believed to be coreleased with glutamate and to modulate glutamatergic synaptic transmission (4, 5). Despite this recent finding, however, much remains to be understood about the dynamics and functional roles of synaptic Zn^{2+}.

Numerous fluorescent Zn^{2+} probes have been developed for use in biological systems (6, 7), including 6-methoxy-(8-*p*-toluenesulfonamido)quinoline (8), Zinquin (9), Zinbo-5 (10), and the Zinpyr (ZP) and ZnAF families of probes (11–14). Despite the abundance of fluorescent Zn^{2+} probes, analysis of Zn^{2+} in vivo remains problematic. Many probes bind Zn^{2+} to form complexes with dissociation constants in the nanomolar range; these tight binding affinities lead to rates of Zn^{2+} release that are too slow for time-resolvable measurements. These probes also may act as Zn^{2+} traps, sequestering Zn^{2+} in one region of the cell, and then collecting elsewhere to yield a faulty image of native Zn^{2+} distributions within cells. Reductions in binding affinity can be accomplished via two strategies. First, steric bulk can be installed near the chelating atoms, as was done with two series of methylated Zn^{2+} probes (15, 16). Second, chelating atoms can be removed from the ligand systematically, as was done for probes in the ZnAF series (16), as well as those in the QZ, Zinspy, and ZinAlkylPyr (ZAP) families (17–19).

Here we present the synthesis of the probe ZinAlkylPyr-4 (ZAP4) and its 6-carboxylic acid derivative (6-CO_2H-ZAP4). The molecular structure of ZAP4 was modeled after earlier ZAP probes (17), with pentafluorobenzyl groups chosen as the alkyl groups to reduce the basicity of the probe and minimize proton-induced enhancement of the emission. The 6-CO_2H-ZAP4 probe was constructed as a membrane-impermeant Zn^{2+} probe, analogous to the previously reported 6-CO_2H-ZP1 (20).

Previous attempts to monitor presynaptic Zn^{2+} dynamics in living brain tissues used membrane-permeant probes to detect intracellular Zn^{2+} from populations of presynaptic terminals at relatively low spatial resolution at the tissue level (21, 22). In addition, activity-dependent extracellular Zn^{2+} release has been monitored with membrane-impermeant probes (16, 23–30). These tissue level-averaged Zn^{2+} imaging methods have limited spatial and temporal resolution and fail to specify the precise location of the relevant synapses.

We describe intracellular Zn^{2+} imaging at the single-synapse level in mossy fiber termini of neurons in acute hippocampal slices from adult mice. The technique relies on the membrane-impermeant fluorescent Zn^{2+} probe 6-CO_2H-ZAP4 and two-photon fluorescence microscopy.

Results

Synthesis and Characterization of ZAP4 and 6-CO_2H-ZAP4. To image the Zn^{2+} within single presynaptic structures, we first synthesized ZAP4 and its membrane-impermeant derivative 6-CO_2H-ZAP4 (Fig. 1*A* and *SI Appendix*, Fig. S1). ZAP4 and 6-CO_2H-ZAP4 can be isolated in good yields through Mannich reactions with

Significance

Zinc is essential to various organs, including the liver and brain. In the brain, Zn^{2+} is present at high concentrations and selectively accumulates in the presynaptic vesicles of glutamatergic neurons. Understanding the roles of zinc in these glutamatergic vesicles has been hampered by the inability to visualize zinc accumulation and release at individual synapses. We report a fluorescent zinc-responsive probe and a technique to selectively image mobile zinc in presynaptic vesicles. Using two-photon laser microscopy, we visualized Zn^{2+} at the synaptic level in tissues from adult mouse brains and successfully monitored Zn^{2+} release from individual neurons. Our probe and methodology will allow further studies into how Zn^{2+} regulates synaptic plasticity and other neurologic functions.

Author contributions: J.C.R., S.J.L., and K.O. designed research; M.K., C.R.G., Z.H., J.G., and T.T.L. performed research; M.K., C.R.G., Z.H., and J.G. analyzed data; and M.K., C.R.G., Z.H., J.G., T.T.L., J.C.R., S.J.L., and K.O. wrote the paper.

The authors declare no conflict of interest.

[1]M.K. and C.R.G. contributed equally to this work.

[2]To whom correspondence may be addressed. E-mail: lippard@mit.edu or okamoto@lunenfeld.ca.

This article contains supporting information online at www.pnas.org/lookup/suppl/doi:10.1073/pnas.1405154111/-/DCSupplemental.

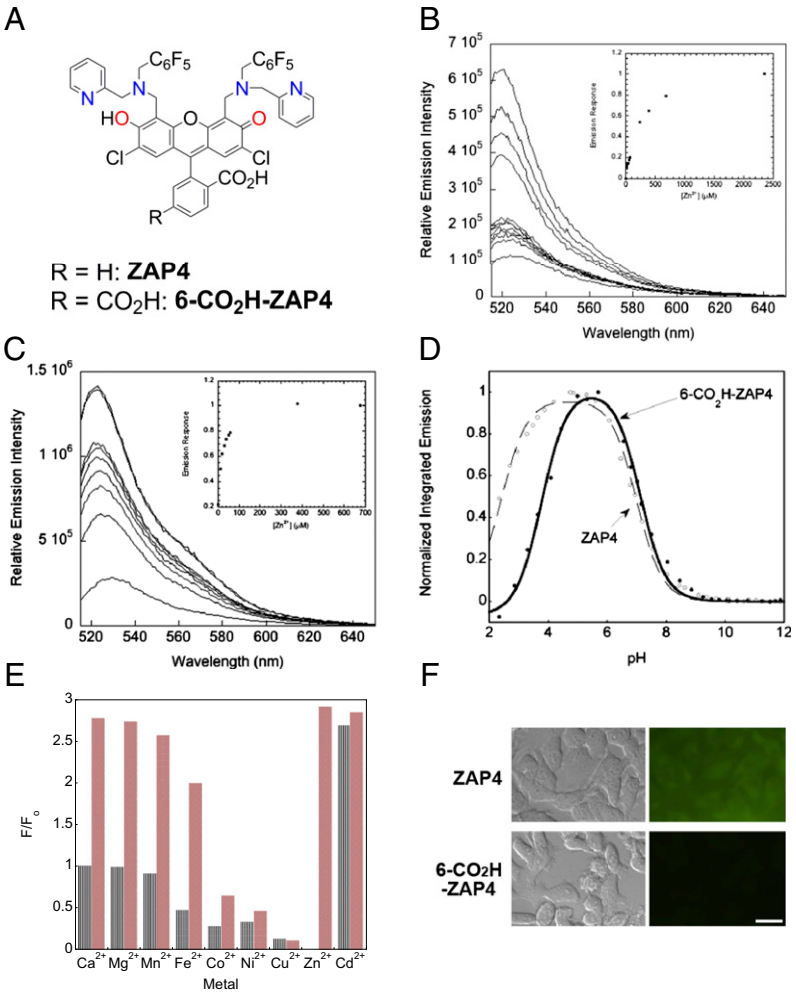

Fig. 1. Properties of Zn^{2+} probes ZAP4 and 6-CO_2H-ZAP4. (*A*) Schematic of the structure of ZAP4 and 6-CO_2H-ZAP4. (*B* and *C*) Fluorescence enhancement of ZAP4 (*B*) and 6-CO_2H-ZAP4 (*C*) probes upon the addition of $ZnCl_2$ in 100 mM KCl, 50 mM Pipes, pH 7.0. (*Insets*) Integrated emission as a function of total Zn^{2+} present. (*B*) The starting concentration of ZAP4 is 1.0 μM, and the concentration of total Zn^{2+} increases to 0, 10, 20, 30, 40, 50, 60, 70, 231, 388, 686, and 2,350 μM. (*C*) The starting concentration of 6-CO_2H-ZAP4 is 1.0 μM, and the concentrations of total Zn^{2+} increase to 0, 10, 20, 30, 40, 50, 60, 378, and 677 μM. (*D*) Normalized integrated emission versus pH for ZAP4 and 6-CO_2H-ZAP4. The fit to the model is shown for each compound. (*E*) Metal ion sensitivity assay for ZAP4. The first bar (gray) is the fluorescent response of 0.5 μM ZAP4 to 100 μM of the listed metal ions at pH 7.0 in 100 mM KCl and 50 mM Pipes. The second bar (red) shows the emission after the addition of 100 μM $ZnCl_2$. All solutions were scanned at 1 min after metal addition. The samples containing Fe^{2+} and Co^{2+} displayed no further emission enhancement, as assessed at 1 h after the addition of zinc ($ZnCl_2$). The responses are normalized to the fluorescence of the free probe (F_0). (*F*) Comparison of HeLa cell fluorescence exposed to ZAP4 (*Upper*) or 6-CO_2H-ZAP4 (*Lower*). (*Left*) Transparent light images. (*Right*) Fluorescence images. Cells were treated with 5 μM of the probe for either 1 h (ZAP4) or 4 h (6-CO_2H-ZAP4). (Scale bar: 100 μm.)

fluorescein precursors that are analogous to the procedures used to prepare ZP1 and ZAP1–3 probes (14, 17). The presence of carboxylic acid on the bottom ring does not appear to affect the synthetic reactions, for the yields of the probes are both ∼60%. The isolation requires no chromatography, and ZAP4 can be crystallized from MeOH and its X-ray structure has been determined, making it the fourth metal-free Zinpyr probe to be structurally characterized to date (31). As with the previously crystallized probes and the Zn_2-ZP1 complex, the bottom carboxylate is locked into the lactone isomer (11, 31). Whether this isomer is the predominant species in solution or whether the lactone formation is a prerequisite for crystal growth is unclear.

Photophysical Characterization of ZAP4 and 6-CO_2H-ZAP4. The maximum absorption and emission wavelengths of metal-free ZAP4 are 514 nm ($\varepsilon = 4{,}650\ M^{-1}\ cm^{-1}$; *SI Appendix*, Fig. S2) and 527 nm ($\phi = 0.19$; Fig. 1*B*), respectively. The low absorptivity compared with other Zn^{2+} probes, such as Zinpyr-1 (ZP1 = 79,500 $M^{-1}\ cm^{-1}$) (11), most likely results from aggregation of the probe. A similarly low absorptivity was observed for ZAP3, a previously reported ZAP probe with phenyl groups in place of the pentafluorophenyl groups (17). On dilution, the ε of the λ_{max} of ZAP3 increased to a value that was more typical of a ZP-type molecule, an observation consistent with the chromophores clustering at high concentrations. We did not observe the same phenomenon for ZAP4, even with the much lower concentrations that could be visualized with a 10-cm path length cuvette.

Upon addition of a large excess of Zn^{2+} (>1 mM $ZnCl_2$), the emission of ZAP4 increased by more than a factor of six (Fig. 1*B*). Concurrently, the absorption and emission wavelengths blue-shifted slightly to 502 nm ($\varepsilon = 8{,}600\ M^{-1}\ cm^{-1}$; *SI Appendix*, Fig. S2) and 520 nm ($\phi = 0.47$; Fig. 1*B*), respectively. After titration by optical spectroscopy, we could distinguish three relevant species: ZAP4, Zn_A-ZAP4, and Zn_B-ZAP4 (*SI Appendix*, Figs. S3 and S4). The metal-ligand stoichiometry of Zn_A-ZAP4 and Zn_B-ZAP4 cannot be assigned with certainty, because these species form only when a large excess of Zn^{2+} is present. Owing to its strong resemblance to ZP1 and other ditopic Zn^{2+}-responsive probes, we speculate that the Zn_A-ZAP4 species is most likely a 2:1 Zn^{2+}-ligand complex, the formation of which is preceded by that of a 1:1 complex that is spectroscopically similar to metal-free ZAP4 (31, 32). The absorption intensity of the Zn_B-ZAP4 species was greater than that of either ZAP4 or Zn_A-ZAP4; it is possible that additional equivalents of Zn^{2+} increase absorption by triggering the dissociation of ZAP4 aggregates. Titrations with $ZnCl_2$ revealed two plateaus in the emission response, one at 30–60 μM and the other at >2 mM zinc (Fig. 1*B*). Of the divalent metal ions tested, only Zn^{2+} and Cd^{2+} induced a fluorimetric enhancement in a 1.0 μM solution of ZAP4. The presence of 100 μM Mg^{2+}, Ca^{2+}, or Mn^{2+} did not significantly alter the fluorimetric response to Zn^{2+} (Fig. 1*E*).

The 6-CO_2H-ZAP4 probe had absorption maxima at 516 nm ($\varepsilon = 60{,}600\ M^{-1}\ cm^{-1}$) and 336 nm ($\varepsilon = 7{,}050\ M^{-1}\ cm^{-1}$) in 100 mM KCl and 50 mM Pipes (pH 7.0). The presence of the carboxylic acid on the bottom ring increased the probe absorptivity significantly,

possibly by disrupting sensor aggregation (17). The 6-CO_2H-ZAP4 excitation maximum of 516 nm is similar to that of the 515-nm band observed for ZP1 (79,500 M^{-1} cm^{-1}) (11). Upon addition of a large excess (>1 mM) of $ZnCl_2$, the fluorescence of 6-CO_2H-ZAP4 increased by more than fivefold (Fig. 1*C*). The 516-nm absorption band shifted to 504 nm upon the addition of $ZnCl_2$, with only a slight decrease in intensity. The quantum yield increased from 0.14 to 0.62 upon saturation with Zn^{2+}. The emission peak shifted from 527 nm to 523 nm (Fig. 1*C*). The spectroscopic changes can be plausibly assigned to the formation of a 2:1 Zn^{2+}–6-CO_2H-ZAP4 complex.

Determination of Probe Affinities for Zn^{2+}. Deconvolution of the changes occurring in both the optical and fluorescence spectra of ZAP4 upon Zn^{2+} chelation yielded dissociation constants (K_d) of 23 ± 7 μM for Zn_A-ZAP4 and 0.54 ± 0.15 mM for Zn_B-ZAP4 (*SI Appendix*, Fig. S2). The overlap of the two binding events precludes more accurate measurement of the K_d value associated with the Zn_A-ZAP4 complex. Stopped-flow kinetic analysis of the first visualizable metal binding event finds a linear correlation between the observed rate constant (k_{obs}) and the concentration of Zn^{2+}, with a $k_2 = 3.07 \pm 0.18 \times 10^5$ M^{-1} s^{-1} at 4.3 °C (*SI Appendix*, Fig. S7). The rate constant associated with the Zn^{2+} dissociation from the 2:1 species was 6.6 ± 2.0 s^{-1}. The K_d value of 22 ± 7 μM calculated from the two rate constants closely agrees with that obtained from the $ZnCl_2$ titrations at 25 °C. The 6-CO_2H derivative 6-CO_2H-ZAP4 differs substantially from ZAP4, exhibiting only a single photophysical response when monitored fluorimetrically. The associated K_d value of 22 ± 4 μM is equal within the limits of error to that found for the formation of Zn_A-ZAP4 from ZAP4 (*SI Appendix*, Fig. S4).

Impact of pH on Probe Emission. As with previous probes with similar structures (11, 17), the emission of ZAP4 and 6-CO_2H-ZAP4 increased as the pH decreased from 12 to 5 (Fig. 1*D*). The fluorescence then decreased as the pH dropped from 5 to 2, a phenomenon associated with protonation of the benzoate ring carboxylate functionalities. The pH dependence of the emission was fit to a two-event model. The pK_a value associated with the increase in fluorescence was 7.00 ± 0.10 for ZAP4 and 7.12 ± 0.10 for 6-CO_2H-ZAP4, both more than 1 unit less than the 8.4 value for ZP1 (11) and almost 1 unit less than the 7.88 for nonfluorinated ZAP3 (17). The pK_a values associated with the acid-induced turnoff were 2.42 ± 0.10 for ZAP4 and 3.77 ± 0.10 for 6-CO_2H-ZAP4.

Two-Photon Properties of 6-CO_2H-ZAP4 for Vesicular Zn^{2+} Imaging in Hippocampal Slices. We evaluated the ability of 6-CO_2H-ZAP4 to image Zn^{2+} in living brain tissues and compared it with the membrane-permeant ZP1, which was used previously to study olfactory bulb tissues (21). We first examined the excitation profiles using two-photon microscopy, which allows for fluorescent imaging of thicker living tissues (33). ZP1 solutions displayed two relatively weak excitation peaks at <700 nm and >1,000 nm in the absence of Zn^{2+} (Fig. 2*A*, no Zn^{2+}). After the addition of 100 μM $ZnCl_2$, the fluorescence intensity increased substantially for all excitation wavelengths from 700 to 1,000 nm (Fig. 2*A*, 100 μM $ZnCl_2$). The 6-CO_2H-ZAP4 probe had a similar two-photon excitation profile in the absence of Zn^{2+} and displayed enhanced fluorescence emission after the addition of 100 μM $ZnCl_2$ (Fig. 2*B*).

To test the ability of these Zn^{2+} probes to function as sensors in brain tissue, we incubated acute hippocampal slices from the brains of adult mice with ZP1 (25 μM) or 6-CO_2H-ZAP4 (5 μM), washed out the excess probe, and then fluorimetrically imaged regions remote from the mossy fibers in the slices (Fig. 2*C*). The tissue background two-photon excitation profiles for emission after application of both ZP1 and 6-CO_2H-ZAP4 were similar and minimal at 850–900 nm; thus, we selected 860 nm as the excitation wavelength for imaging Zn^{2+} in brain slices.

Visualization of Presynaptic Zn^{2+} at the Hippocampal Mossy Fiber Termini of Adult Acute Slices. To image endogenous, presynaptic Zn^{2+} in mossy fiber termini, we incubated acutely prepared hippocampal slices with membrane-permeant ZP1. Intense fluorescent staining revealed the hilus of the dentate gyrus (DG) and the CA3 stratum lucidum in the mossy fiber region (Fig. 2*D*, *Upper*).

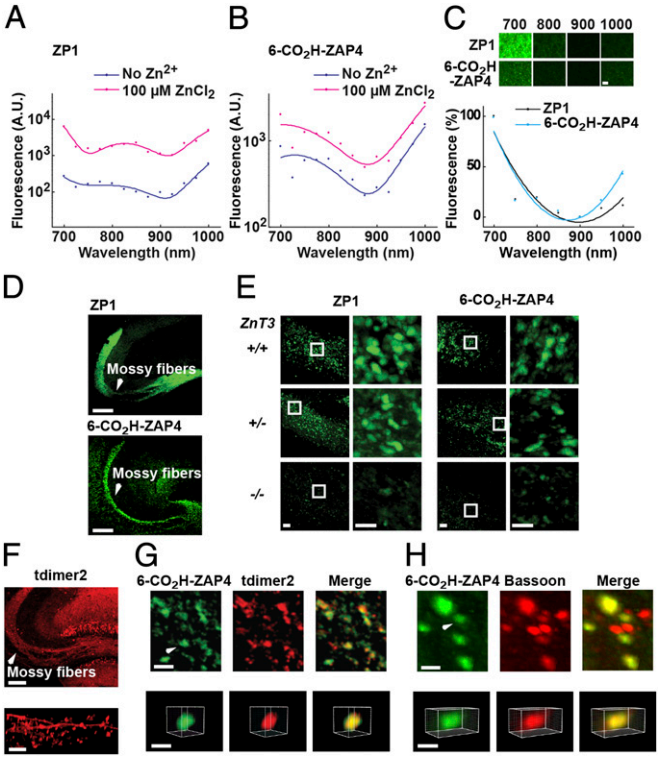

Fig. 2. Visualization of presynaptic Zn^{2+} in hippocampal mossy fiber termini with Zn^{2+} probes. (*A* and *B*) In vitro two-photon excitation profiles of Zn^{2+} probes in the absence (blue) and presence (magenta) of 100 μM $ZnCl_2$. The dots represent average fluorescence intensity (n = 3). The Zn^{2+} probe solutions, ZP1 (*A*; 25 μM) and 6-CO_2H-ZAP4 (*B*; 5 μM), were prepared in 50 mM Pipes and 100 mM KCl (pH 7). The emission wavelength for fluorescence detection was 495–540 nm. (*C*, *Upper*) Images from acutely isolated mouse hippocampal slices showing background levels of Zn^{2+} probe ZP1 (25 μM) and 6-CO_2H-ZAP4 (5 μM) fluorescence using various two-photon excitation wavelengths. (Scale bar: 5 μm.) (*Lower*) Slices were stained for 10 min, and the fluorescence intensity in the region surrounding the mossy fibers in the slices was measured and plotted. (*D*) Representative images of Zn^{2+} stained mossy fiber regions in hippocampal slices. Acute adult mouse hippocampal slices were stained with ZP1 (25 μM) or 6-CO_2H-ZAP4 (5 μM). (Scale bars: 200 μm.) (*E*) Zn^{2+} probe fluorescence images in mossy fiber region of adult wild type (WT; $^{+/+}$), *ZnT3* heterozygous ($^{+/-}$), and *ZnT3* null ($^{-/-}$) mice. The white squares on images on the left represent the enlarged regions shown in the corresponding image on the right. (Scale bars: *Left*, 10 μm; *Right*, 5 μm.) (*F*, *Upper*) Fluorescent images of the mossy fiber region sparsely expressing red fluorescence (tdimer2) in adult hippocampal slices (Thy1-Brainbow 1.0 line H transgenic mouse). (*Lower*) Images of red fluorescent mossy fibers including boutons in the hippocampal slice. (Scale bars: *Upper*, 100 μm; *Lower*, 10 μm.) (*G*, *Upper*) Colocalization of 6-CO_2H-ZAP4 (green) and tdimer2 (red) in mossy fiber boutons of a hippocampal slice. (*Lower*) Enlarged, 3D view of the mossy fiber boutons indicated by a white arrow. (Scale bars: *Upper*, 5 μm; *Lower*, 2 μm.). (*H*, *Upper*) Colocalization of 6-CO_2H-ZAP4 (green) and a presynaptic active zone marker, bassoon (red), in a hippocampal slice. (*Lower*) Enlarged, 3D view of the boutons indicated by a white arrow. Presynaptic structures were immunolabeled by bassoon antibody after staining with 6-CO_2H-ZAP4. (Scale bars: *Upper*, 2 μm; *Lower*, 2 μm.)

The membrane-impermeant probe 6-CO_2H-ZAP4 was loaded into bouton presynaptic vesicles through a protocol similar to that used for the lipophilic membrane probe FM1-43 (34, 35). Slices were immersed in artificial cerebrospinal fluid (ACSF) containing 5 μM 6-CO_2H-ZAP4 and 45 mM KCl for 15 min, which induces fusion of synaptic vesicles with the presynaptic membrane that are subsequently recycled and replenished with Zn^{2+} and other vesicular content. The 6-CO_2H-ZAP4 is endocytosed during this process, becoming trapped within the newly formed synaptic vesicles because of its membrane impermeability. Excess 6-CO_2H-ZAP4 was removed by continuous perfusion with ACSF for at least 10 min. Two-photon fluorescence imaging of the slice revealed high accumulation of 6-CO_2H-ZAP4 in the stratum lucidum layer between the CA3 and DG relative to other hippocampal regions (Fig. 2*D*, *Lower*). The discontinuous mossy fiber staining is more evident in the higher-magnification images containing discrete puncta that most likely represent active boutons with Zn^{2+} accumulation in their synaptic vesicles (Fig. 2*E*, *Top*).

To confirm that the puncta report Zn^{2+}, we applied the probes to brain slices obtained from zinc transporter 3 (ZnT3) knockout mice (36), which lack vesicular synaptic zinc (Fig. 2*E*, *Middle* and *Bottom*). Both ZP1 and 6-CO_2H-ZAP4 produced fluorescent puncta in the mossy fiber regions of $ZnT3^{+/+}$ and $ZnT3^{+/-}$ hippocampal slices, whereas staining was reduced in $ZnT3^{-/-}$ hippocampi to a similar intensity as in other hippocampal subregions.

We also examined the distribution of 6-CO_2H-ZAP4 fluorescent puncta in Thy1-Brainbow1.0 (line H) mice (37) that express a red fluorescent protein (tdimer2) in mossy fiber boutons. In slices from the Brainbow mice, neurons exhibiting sparse red fluorescence were detected in DG granule neurons and their mossy fiber axons (Fig. 2*F*). After treatment with 6-CO_2H-ZAP4, we detected some of the 6-CO_2H-ZAP4 fluorescent puncta (green) overlapped with red spots in the mossy fiber region (Fig. 2*G*, *Upper*); higher-magnification 3D images revealed colocalized puncta of 6-CO_2H-ZAP4 and tdimer2 (Fig. 2*G*, *Lower*). To confirm whether the 6-CO_2H-ZAP4 puncta are localized in presynaptic regions, we immunostained hippocampal slices with the presynaptic active zone marker bassoon (38) after staining with 6-CO_2H-ZAP4 (Fig. 2*H*). The 6-CO_2H-ZAP4 puncta were preserved even after fixation and permeabilization. The puncta overlapped with bright bassoon spots, indicating presynaptic localization of the 6-CO_2H-ZAP4 probe.

The addition of the membrane-permeant Zn^{2+} chelator tris-(2-pyridylmethyl)amine (TPA) (21) reduced the fluorescence intensity of both ZP1 and 6-CO_2H-ZAP4 puncta compared with control slices continuously perfused with ACSF alone, indicating that both probes report Zn^{2+} within boutons that contain synaptic vesicles (Fig. 3 *A* and *B*). These results demonstrate that both membrane-permeant ZP1 and membrane-impermeant 6-CO_2H-ZAP4 detect accumulated Zn^{2+} within the vesicles of mossy fiber boutons from acutely prepared hippocampal slices of adult mice.

Visualization of Activity-Dependent Release of Zn^{2+} at the Mossy Fiber Termini of Adult Acute Slices. To monitor activity-dependent Zn^{2+} release in mossy fiber boutons, we first loaded synaptic vesicles with the zinc probes. The fluorescence intensity of ZP1-stained boutons dropped (by 1.1% per min) during continuous perfusion of ACSF (Fig. 3*C*), but was unaffected by a K^+-evoked depolarizing stimulus (ACSF containing 90 mM KCl for 90 s). In contrast, 6-CO_2H-ZAP4–stained puncta maintained their fluorescence signal during perfusion and showed a large K^+-evoked reduction in fluorescence intensity (Fig. 3*D*). The fluorescence intensity change was largely blocked by application of (2*S*,2′*R*,3′*R*)-2-(2′,3′-dicarboxycyclopropyl)glycine (DCG-IV), a mGluR2/3 agonist that modulates mossy fiber neurotransmitter release (39–41). The mGluR2-mediated suppression of the K^+-evoked response suggests that the change in 6-CO_2H-ZAP4 fluorescence intensity is concomitant with transmitter release from the mossy fiber boutons.

We next evaluated whether the trapped 6-CO_2H-ZAP4 can be released from synaptic vesicles through electrical stimulation of the mossy fibers. A fine glass electrode was placed 5–15 μm

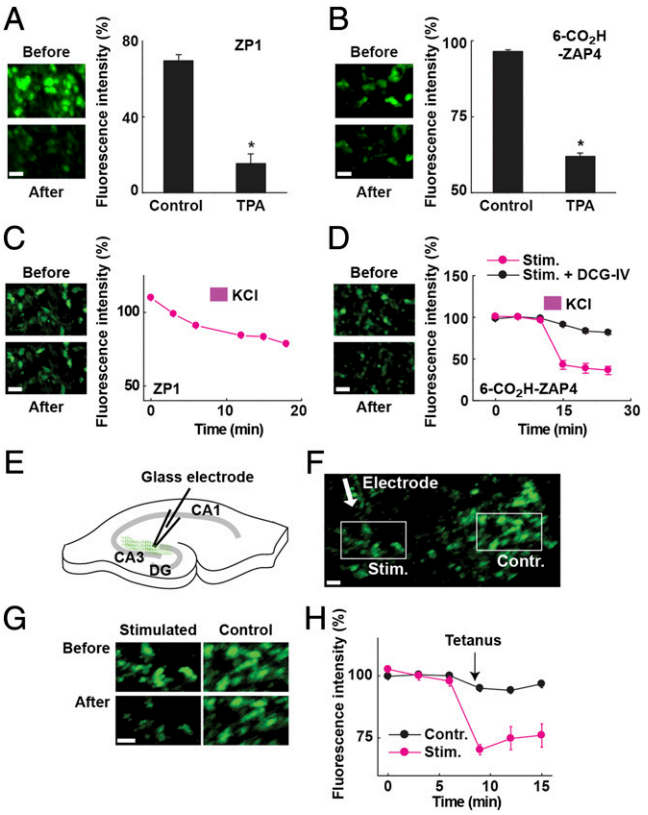

Fig. 3. Synaptic activity-dependent release of Zn^{2+} at mossy fiber termini. (*A* and *B*, *Left*) Representative Zn^{2+} probe fluorescence images in slices stained with ZP1 (*A*) or 6-CO_2H-ZAP4 (*B*). Images were obtained before (Before) and 10 min after (After) TPA treatment. (Scale bar: 5 μm.) (*Right*) Quantification of Zn^{2+} chelator-dependent fluorescence intensity changes in mossy fiber boutons stained with ZP1 (*A*) and 6-CO_2H-ZAP4 (*B*). The fluorescent intensity changes were measured with or without TPA treatment of the hippocampal slices. ZP1: control, $n = 14$; TPA, $n = 10$; 6-CO_2H-ZAP4: control, $n = 9$; TPA, $n = 15$. The stained slices were perfused for 10 min with ACSF (control) or 200 μM TPA (TPA). *$P < 0.01$, paired *t* test. (*C* and *D*, *Left*) Representative Zn^{2+} fluorescent images in slices stained with ZP1 (*C*) or 6-CO_2H-ZAP4 (*D*). Images were collected before (Before) and immediately after (After) a K^+-evoked depolarizing stimulus (ACSF containing 90 mM KCl for 90 s). (Scale bar: 5 μm.) (*Right*) Time course of the Zn^{2+} fluorescence intensity change in mossy fiber termini, normalized to the average intensity before the K^+-evoked depolarizing stimulus (magenta bar). DCG-IV (5 μM) was added in ACSF after 6-CO_2H-ZAP4 staining (Stim. + DCG-IV). ZP1 ($n = 18$), 6-CO_2H-ZAP4 (Stim.; $n = 8$), 6-CO_2H-ZAP4 + DCG-IV (Stim. + DCG-IV; $n = 14$). (*E*) Schematic drawing of the configuration for local tetanic electrical stimulation using a glass electrode in the slice. (*F*) Fluorescence image from a mossy fiber region of a living hippocampal slice stained with 6-CO_2H-ZAP4. The arrow represents the position of the inserted electrode tip. The mossy fiber regions in white squares near the electrode (Stim.) and control regions at a distance from the electrode (Contr.) are enlarged in *G*. (Scale bar: 5 μm.) (*G*) 6-CO_2H-ZAP4 fluorescence at two mossy fiber regions obtained before and immediately after tetanic stimulation. (Scale bar: 5 μm.) (*H*) Time course of the fluorescence intensity averaged from boutons and normalized to prestimulation levels. Control (Contr.; black circles; $n = 8$): mossy fiber region >30 μm away from stimulation points (glass electrode). Stimulation (Stim.; magenta circles; $n = 8$): mossy fiber region 5–15 μm (stimulation range) away from the electrode.

from a cluster of labeled boutons. On local tetanic electrical stimulation (42, 44) (Fig. 3*E*), 6-CO_2H-ZAP4 emissions were decreased at regions near the electrode (stimulated), but not at distant sites (control) within the same slices (Fig. 3 *F–H*). These results reveal that 6-CO_2H-ZAP4 monitors activity-dependent Zn^{2+} release from mossy fiber boutons.

Discussion

Development of Zn^{2+} Probes. The ZAP4 and 6-CO_2H-ZAP4 probes were designed to be less-basic analogs of previously reported ZAP sensors (17). The higher basicity of those sensors precluded them from detecting Zn^{2+} at neutral pH. The target compounds were synthesized through well-established steps and can be isolated in good yields without chromatography.

The ZAP4 sensor has a notably low molar extinction coefficient for the main feature at 514 nm (ε = 4,650 M^{-1} cm^{-1}). The next-weakest major band among Zinpyr-type fluorescein probes is that of ZAP3 (510 nm; ε = 23,700 M^{-1} cm^{-1}) (17). Derivatives of fluorescein that enforce lactone formation are commonly colorless. The ability to crystallize this form of the metal-free probe may indicate a larger portion of this isomer in solution, which would explain its weak absorbance. Alternatively, aggregation of the sensor in solution may affect absorbance; a similar process is suspected to occur for ZAP3 (17), which exhibits a higher ε value at lower concentrations. Curiously, 6-CO_2H-ZAP4 has a much stronger band at 516 nm (ε = 60,600 M^{-1} cm^{-1}) compared with ZAP4; otherwise, the photophysical features, particularly the quantum yields of the metal-free and Zn^{2+}-saturated forms, are similar.

The similarity extends to the basicities of the metal-free probes and the dissociation constants associated with the first observable Zn^{2+}-binding event, and the carboxylic acid installed on the bottom ring of 6-CO_2H-ZAP4 does not appear to affect the cation-binding properties of the two metal-binding domains. The pK_a values for the proton-induced turn-on for ZAP4 and 6-CO_2H-ZAP4 are within the limits of error of each other. The pentafluorbenzyl substituents successfully decrease these values relative to those reported for ZAP1-3, and enable fluorimetric Zn^{2+} detection at pH 7.0 (22). The binding affinities associated with the first observable Zn^{2+}-binding event are also identical within the limits of error of each other. The fluorescence responses likely correspond to the formation of 2:1 Zn^{2+}-ligand complexes, given that metallation of both metal-binding domains was required for the emissive response in previously described ditopic Zn^{2+} sensors (31, 32). In these systems, the 1:1 Zn^{2+}-ligand complex was too spectroscopically similar to the metal-free probe to allow observation by a simple fluorimetric titration. The K_d values for the 2:1 Zn^{2+}-ligand complexes of ZAP4 (23 μM) and 6-CO_2H-ZAP4 (22 μM) are similar in magnitude to those measured for the QZ family (18).

Stopped-flow kinetic studies on the first observable association reaction between ZAP4 and Zn^{2+} suggest a first-order dependence on the metal ion, and the reaction is most simply interpreted as a bimolecular collision. The equilibrium constant measured from the forward and backward rates agrees well with that obtained from singular value decomposition analysis of the titrations. The rate constant associated with the dissociation is greater than those measured for ZP1 probes, but less than those measured for QZ probes, as is the rate of Zn^{2+} release (18).

The rapid metal ion release renders the probe less susceptible to metal contamination, much like the QZ and Zinspy probes (18, 19) and, to a lesser extent, the Me_4ZP1 probe (15). The ZAP4 sensor is capable of detecting Zn^{2+} in the presence of an equimolar concentration of Fe^{2+}. Equimolar concentrations of Co^{2+}, Ni^{2+}, and Cu^{2+} prevent the emission from exceeding that of the metal-free probe. The very low cellular concentrations of these free ions should not affect biological imaging with ZAP4 and 6-CO_2H-ZAP4.

Based on their K_d values and significant fluorescent responses to Zn^{2+}, these probes have a potential use in quantifying cellular Zn^{2+} concentrations. However, the membrane-permeant ZAP4 has a sluggish second binding event, which can complicate interpretation of the fluorescence response. Moreover, the much weaker absorption of ZAP4 severely limits the brightness of its emission and thus its applicability to the study of biological processes. Conversely, the membrane-impermeant 6-CO_2H-ZAP4 has a single photophysical response for Zn^{2+} and a much stronger absorption maximum than ZAP4.

Application of Zn^{2+} Probes in Adult Mouse Acute Hippocampal Slices. The ability of 6-CO_2H-ZAP4 to successfully image synaptic vesicle Zn^{2+} in the mossy fiber boutons of hippocampal neurons with two-photon fluorescence microscopy has several important implications. Two-photon fluorescence microscopy enables deep-tissue Zn^{2+} imaging and avoids imaging nonspecific fluorescence on the slice surface. The Zn^{2+} images displayed here are of sufficiently high resolution for tracking individual synaptic termini. Because 6-CO_2H-ZAP4 is membrane-impermeant, its introduction into synaptic vesicles requires neuronal depolarization, with the probe entering the vesicles during the subsequent recycling event (Fig. 4*A*). The resultant bright fluorescence signal may be somewhat enhanced by proton-induced probe turn-on within the acidic vesicles (~pH 5), the contribution of which can be estimated by the results from the described *ZnT3* knockout mouse study.

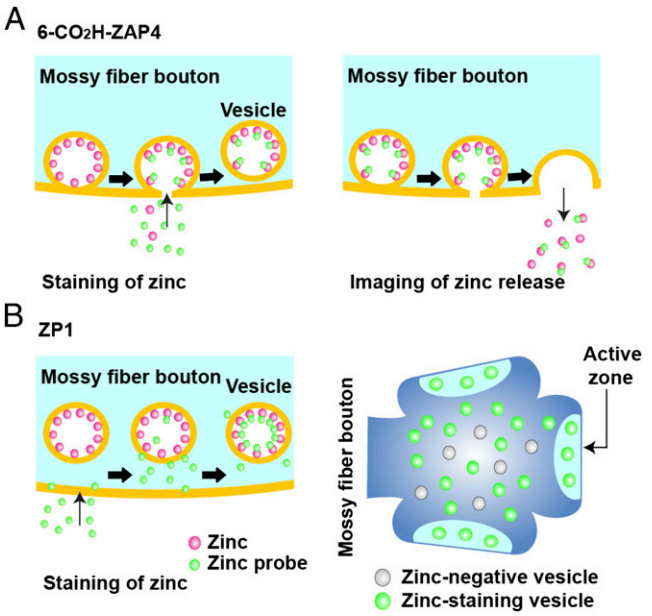

Fig. 4. Models for presynaptic Zn^{2+} imaging method at mossy fiber termini using Zn^{2+} probes. (*A*, *Left*) Schematic model of presynaptic vesicle Zn^{2+} staining using a membrane-impermeant Zn^{2+} probe. Weak depolarization stimulus induces fusion of some synaptic vesicles that allows membrane-impermeant 6-CO_2H-ZAP4 to enter into the fused vesicles. The fluorescence probe then binds to Zn^{2+} concentrated within vesicles by Zn^{2+} transporters localized to the vesicle membrane. (*Right*) Schematic model of Zn^{2+} release in mossy fiber termini during electric stimulation. Tetanic stimulation induces full-collapse fusion events of synaptic vesicles into the bouton membrane which is sufficient to release a large proportion of Zn^{2+} (along with the fluorescent probe) from synaptic vesicles. (*B*) Model for Zn^{2+} staining with the cell membrane-permeant fluorescence probe in mossy fiber termini. (*Left*) The Zn^{2+} probe (ZP1) stains Zn^{2+} within vesicles without synaptic activation owing to its membrane permeability. (*Right*) The membrane-permeant probe ZP1 stains Zn^{2+}-containing vesicles throughout the mossy fiber bouton. The mossy fiber bouton contains multiple active zones (cyan region).

The mossy fiber bouton is quite large (2–5 μm diameter) and contains ~16,000 synaptic vesicles (43). Synaptic activation most likely releases only a limited number of these vesicles, perhaps mainly near active zones. The ZP1 probe is membrane-permeant and able to stain all Zn^{2+}-containing vesicles (Fig. 4*B*). This property effectively reduces its sensitivity in detecting Zn^{2+} dynamics and limits its use solely to the detection of the massive Zn^{2+} release expected during strong electric stimulation in tissue-level assays (21). However, for synapse-level Zn^{2+} imaging, local electric stimulation (42, 44) and highly magnified observation optics are needed to measure Zn^{2+}. Because 6-CO_2H-ZAP4 stains Zn^{2+} only in actively recycled vesicles, it may be retained in vesicles near active zones, which are more likely to be released on stimulation. This phenomenon may allow 6-CO_2H-ZAP4 to more efficiently detect release of Zn^{2+} relative to ZP1 and is one likely reason for the discrepancy in the ability of ZP1 and 6-CO_2H-ZAP4 to monitor K^+-evoked Zn^{2+} release. Thus, 6-CO_2H-ZAP4, in combination with two-photon imaging, provides a unique tool for monitoring Zn^{2+} release and dynamics in living tissues at single-synapse resolution. Our method will enable studies of presynaptic Zn^{2+} function in synaptic plasticity, toxicity, and zincopathic brain disease.

Materials and Methods

Materials and procedures for all experiments are described in detail in *SI Appendix*. Included in this appendix are the synthesis and characterization of compounds, neuronal imaging protocols, and two-photon microscopy experiments. Also provided are additional figures and tables relating to the characterization of compounds.

ACKNOWLEDGMENTS. We thank Dr. Datong Song [Massachusetts Institute of Technology (MIT)] for solving the crystal structure of ZAP4 and Dr. Gleb Shumyatsky (Rutgers University) for providing the *ZnT3*$^{+/-}$ mouse. We also thank Dr. Yasunori Hayashi (MIT-RIKEN Brain Science Institute) for assistance in designing the imaging protocol and for his interest in the early stages of this research. This work was supported by the National Institute of General Medical Sciences [Grant GM 65519 (to S.J.L.)], the Natural Sciences and Engineering Research Council of Canada Discovery Grants program (K.O.), Canadian Institutes of Health Research [Grant MOP 111220 (to K.O.)], the Canada Research Chairs Program (K.O.), and the Canada Foundation for Innovation (K.O.). C.R.G. was supported by a postdoctoral fellowship from the National Institutes of Health.

1. Frederickson CJ, Koh J-Y, Bush AI (2005) The neurobiology of zinc in health and disease. *Nat Rev Neurosci* 6(6):449–462.
2. Bush AI (2000) Metals and neuroscience. *Curr Opin Chem Biol* 4(2):184–191.
3. Frederickson CJ, Bush AI (2001) Synaptically released zinc: Physiological functions and pathological effects. *BioMetals* 14(3-4):353–366.
4. Pan E, et al. (2011) Vesicular zinc promotes presynaptic and inhibits postsynaptic long-term potentiation of mossy fiber-CA3 synapse. *Neuron* 71(6):1116–1126.
5. Vogt K, Mellor J, Tong G, Nicoll R (2000) The actions of synaptically released zinc at hippocampal mossy fiber synapses. *Neuron* 26(1):187–196.
6. Chang CJ, Lippard SJ (2006) Zinc metalloneurochemistry: Physiology, pathology, and probes. *Metal Ions in Life Sciences*, eds Sigel A, Sigel H, Sigel RKO (Wiley, Chichester, UK), Vol 1, pp 281–320.
7. Kikuchi K, Komatsu K, Nagano T (2004) Zinc sensing for cellular application. *Curr Opin Chem Biol* 8(2):182–191.
8. Frederickson CJ, Kasarskis EJ, Ringo D, Frederickson RE (1987) A quinoline fluorescence method for visualizing and assaying the histochemically reactive zinc (bouton zinc) in the brain. *J Neurosci Methods* 20(2):91–103.
9. Zalewski PD, Forbes IJ, Betts WH (1993) Correlation of apoptosis with change in intracellular labile Zn(II) using Zinquin [(2-methyl-8-p-toluenesulphonamido-6-quinolyloxy)acetic acid], a new specific fluorescent probe for Zn(II). *Biochem J* 296(Pt 2): 403–408.
10. Taki M, Wolford JL, O'Halloran TV (2004) Emission ratiometric imaging of intracellular zinc: Design of a benzoxazole fluorescent sensor and its application in two-photon microscopy. *J Am Chem Soc* 126(3):712–713.
11. Burdette SC, Walkup GK, Spingler B, Tsien RY, Lippard SJ (2001) Fluorescent sensors for Zn^{2+} based on a fluorescein platform: Synthesis, properties and intracellular distribution. *J Am Chem Soc* 123(32):7831–7841.
12. Chang CJ, et al. (2004) ZP8, a neuronal zinc sensor with improved dynamic range; imaging zinc in hippocampal slices with two-photon microscopy. *Inorg Chem* 43(21): 6774–6779.
13. Hirano T, Kikuchi K, Urano Y, Nagano T (2002) Improvement and biological applications of fluorescent probes for zinc, ZnAFs. *J Am Chem Soc* 124(23):6555–6562.
14. Walkup GK, Burdette SC, Lippard SJ, Tsien RY (2000) A new cell-permeable fluorescent probe for Zn^{2+}. *J Am Chem Soc* 122(23):5644–5645.
15. Goldsmith CR, Lippard SJ (2006) 6-Methylpyridyl for pyridyl substitution tunes the properties of fluorescent zinc sensors of the Zinpyr family. *Inorg Chem* 45(2):555–561.
16. Komatsu K, Kikuchi K, Kojima H, Urano Y, Nagano T (2005) Selective zinc sensor molecules with various affinities for Zn^{2+}, revealing dynamics and regional distribution of synaptically released Zn^{2+} in hippocampal slices. *J Am Chem Soc* 127(29): 10197–10204.
17. Goldsmith CR, Lippard SJ (2006) Analogues of Zinpyr-1 provide insight into the mechanism of zinc sensing. *Inorg Chem* 45(16):6474–6478.
18. Nolan EM, et al. (2005) QZ1 and QZ2: Rapid, reversible quinoline-derivatized fluoresceins for sensing biological Zn(II). *J Am Chem Soc* 127(48):16812–16823.
19. Nolan EM, Lippard SJ (2004) The Zinspy family of fluorescent zinc sensors: Syntheses and spectroscopic investigations. *Inorg Chem* 43(26):8310–8317.
20. Woodroofe CC, Masalha R, Barnes KR, Frederickson CJ, Lippard SJ (2004) Membrane-permeable and -impermeable sensors of the Zinpyr family and their application to imaging of hippocampal zinc in vivo. *Chem Biol* 11(12):1659–1666.
21. Blakemore LJ, Tomat E, Lippard SJ, Trombley PQ (2013) Zinc released from olfactory bulb glomeruli by patterned electrical stimulation of the olfactory nerve. *Metallomics* 5(3):208–213.
22. Takeda A, et al. (2011) Transient increase in Zn^{2+} in hippocampal CA1 pyramidal neurons causes reversible memory deficit. *PLoS ONE* 6(12):e28615.
23. Budde T, Minta A, White JA, Kay AR (1997) Imaging free zinc in synaptic terminals in live hippocampal slices. *Neuroscience* 79(2):347–358.
24. Kay AR (2003) Evidence for chelatable zinc in the extracellular space of the hippocampus, but little evidence for synaptic release of Zn. *J Neurosci* 23(17):6847–6855.
25. Kay AR, Tóth K (2006) Influence of location of a fluorescent zinc probe in brain slices on its response to synaptic activation. *J Neurophysiol* 95(3):1949–1956.
26. Koyama R, Yamada MK, Nishiyama N, Matsuki N, Ikegaya Y (2002) Group II metabotropic glutamate receptor activation is required for normal hippocampal mossy fibre development in the rat. *J Physiol* 539(Pt 1):157–162.
27. Li Y, Hough CJ, Suh SW, Sarvey JM, Frederickson CJ (2001) Rapid translocation of Zn^{2+} from presynaptic terminals into postsynaptic hippocampal neurons after physiological stimulation. *J Neurophysiol* 86(5):2597–2604.
28. Qian J, Noebels JL (2005) Visualization of transmitter release with zinc fluorescence detection at the mouse hippocampal mossy fibre synapse. *J Physiol* 566(Pt 3):747–758.
29. Takeda A, et al. (2006) Zinc release from Schaffer collaterals and its significance. *Brain Res Bull* 68(6):442–447.
30. Ueno S, et al. (2002) Mossy fiber Zn^{2+} spillover modulates heterosynaptic N-methyl-D-aspartate receptor activity in hippocampal CA3 circuits. *J Cell Biol* 158(2):215–220.
31. Wong BA, Friedle S, Lippard SJ (2009) Solution and fluorescence properties of symmetric dipicolylamine-containing dichlorofluorescein-based Zn^{2+} sensors. *J Am Chem Soc* 131(20):7142–7152.
32. Buccella D, Horowitz JA, Lippard SJ (2011) Understanding zinc quantification with existing and advanced ditopic fluorescent Zinpyr sensors. *J Am Chem Soc* 133(11): 4101–4114.
33. Helmchen F, Denk W (2005) Deep tissue two-photon microscopy. *Nat Methods* 2(12): 932–940.
34. Pyle JL, Kavalali ET, Choi S, Tsien RW (1999) Visualization of synaptic activity in hippocampal slices with FM1-43 enabled by fluorescence quenching. *Neuron* 24(4): 803–808.
35. Stanton PK, Heinemann U, Müller W (2001) FM1-43 imaging reveals cGMP-dependent long-term depression of presynaptic transmitter release. *J Neurosci* 21(19):RC167.
36. Cole TB, Wenzel HJ, Kafer KE, Schwartzkroin PA, Palmiter RD (1999) Elimination of zinc from synaptic vesicles in the intact mouse brain by disruption of the ZnT3 gene. *Proc Natl Acad Sci USA* 96(4):1716–1721.
37. Livet J, et al. (2007) Transgenic strategies for combinatorial expression of fluorescent proteins in the nervous system. *Nature* 450(7166):56–62.
38. tom Dieck S, et al. (1998) Bassoon, a novel zinc-finger CAG/glutamine-repeat protein selectively localized at the active zone of presynaptic nerve terminals. *J Cell Biol* 142(2):499–509.
39. Ishida M, Saitoh T, Shimamoto K, Ohfune Y, Shinozaki H (1993) A novel metabotropic glutamate receptor agonist: Marked depression of monosynaptic excitation in the newborn rat isolated spinal cord. *Br J Pharmacol* 109(4):1169–1177.
40. Kamiya H, Shinozaki H, Yamamoto C (1996) Activation of metabotropic glutamate receptor type 2/3 suppresses transmission at rat hippocampal mossy fibre synapses. *J Physiol* 493(Pt 2):447–455.
41. Nicholls RE, et al. (2006) mGluR2 acts through inhibitory Gα subunits to regulate transmission and long-term plasticity at hippocampal mossy fiber-CA3 synapses. *Proc Natl Acad Sci USA* 103(16):6380–6385.
42. Okamoto K, Nagai T, Miyawaki A, Hayashi Y (2004) Rapid and persistent modulation of actin dynamics regulates postsynaptic reorganization underlying bidirectional plasticity. *Nat Neurosci* 7(10):1104–1112.
43. Rollenhagen A, Lübke JHR (2010) The mossy fiber bouton: The "common" or the "unique" synapse? *Front Synaptic Neurosci* 2:2.
44. Shi S-H, et al. (1999) Rapid spine delivery and redistribution of AMPA receptors after synaptic NMDA receptor activation. *Science* 284(5421):1811–1816.